Earth and Planetary Science Letters 554 (2021) 116695

Contents lists available at ScienceDirect

Earth and Planetary Science Letters

www.elsevier.com/locate/epsl

Geometrically controlled slow slip enhanced by seismic waves: A mechanism for delayed triggering

David Blank [a,*], Julia Morgan [a], Yannick Caniven [a,b]

[a] Rice University, 6100 Main Street, Houston, TX 77005, United States of America
[b] University of Montpellier, CNRS France, 641 Av. Du Doyen Gaston Giraud, 34000 Montpellier, France

ARTICLE INFO

Article history:
Received 22 May 2020
Received in revised form 20 November 2020
Accepted 22 November 2020
Available online 4 December 2020
Editor: R. Bendick

Keywords:
delayed dynamic triggering
slow slip
numerical modeling
earthquakes

ABSTRACT

Seismic waves generated during earthquakes induce transient stress changes in the crust. These ephemeral perturbations can trigger critically stressed asperities at remote distances, often with significant time delays. The physical mechanism that governs this phenomenon is not completely resolved. Numerical simulations of dynamic perturbations passing along a heterogeneous pre-stressed fault, demonstrate that weak portions of the fault that host ongoing slow slip can transfer stress in response to the perturbations, loading asperities poised for failure. We find that the magnitude of perturbation, the state of the asperity, as well as deformation of the surrounding material, jointly control the delay time between perturbation and triggered event. The slow-slip modulated delayed triggering model that we propose can account for the wide range of observed delay times in nature, including the two end-member cases of no delay and no triggering. Triggered slow slip events in nature might provide warning signs of impending earthquakes, underscoring the importance of high-resolution monitoring of active fault zones.

© 2020 Elsevier B.V. All rights reserved.

1. Introduction

Large earthquakes often take place in spatiotemporal bursts. When the separation in time and space between these earthquakes is very low, we recognize them as foreshock, mainshock, and aftershock sequences. However, some earthquake pairs are separated by unusually large time and distance gaps. The low statistical likelihood that such events are simply coincidental suggests a causal relationship, for example, earthquake triggering [Freed, 2005]. A better understanding of the physical mechanisms that control this relationship can improve seismic hazard assessment of triggered seismicity.

Two basic mechanisms for triggered seismicity are commonly invoked to explain the phenomenon. (1) Redistribution of static stresses in the earth that accompany earthquakes can increase the likelihood of failure on faults that lie in zones of stress rise [King et al., 1994; Stein, 1999; Kilb et al., 2002]. Because static stress change decays rapidly with distance from the rupture, this triggering mechanism cannot account for event pairs that are separated by more than a few fault lengths [Harris, 1998; Stein, 1999; Hodge et al., 2018]. Events that violate this spatial criterion are often explained instead by (2) dynamic triggering, where transient stress changes associated with seismic waves might push a fault to failure [Hill et al., 1993; Brodsky and van der Elst, 2014; Gomberg et al., 2001, 2003, 2004; Gomberg and Johnson, 2005; Parsons, 2005; Johnson and Bürgmann, 2016; Walter et al., 2015; Wallace et al., 2017]. Both static and dynamic triggering explanations employ straightforward Coulomb failure criteria [Jaeger et al., 1979]. As such, triggering should theoretically take place either instantly or not at all. This is difficult to reconcile with the commonly observed delays between causative and triggered earthquakes.

A case in point is the pair of >M7 earthquakes that struck Mexico in September 2017 (M8.2 September 7 Chiapas and M7.1 September 19 Puebla), which were separated by 650 km in distance and 12 days in time [Alberto et al., 2018]. Static stress changes from the Chiapas event are too small and too local to have triggered the eventual Puebla nucleation zone [Toda and Stein, 2017; Segou and Parsons, 2018]. Dynamic stress perturbations could have triggered the second event; however, it is difficult to explain the 12-day delay. Even more puzzling is the seven-year delay between the M7.3 Landers and M7.1 Hector Mine earthquakes, which have been interpreted to be related [Kilb et al., 2000; Zeng, 2001; Felzer et al., 2002]. These examples suggest that dynamic waves may be capable of triggering failure on critically stressed faults beyond the reach of static stress changes, however, there

* Corresponding author.
E-mail address: dgb3@rice.edu (D. Blank).

https://doi.org/10.1016/j.epsl.2020.116695
0012-821X/© 2020 Elsevier B.V. All rights reserved.

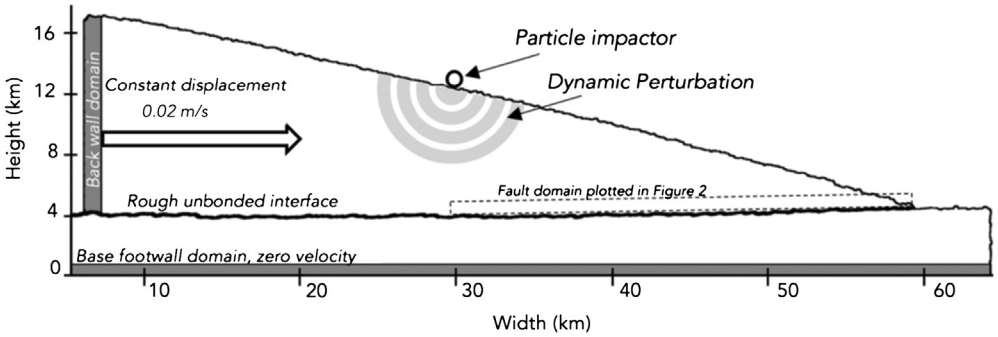

Fig. 1. Model setup. An unbonded, geometrically heterogeneous megathrust fault surface separates the bonded upper and lower particle assemblages. Fixed velocity boundary conditions (gray) drive fault slip. Point source dynamic perturbations are generated by a particle impactor. Dashed box denotes fault slip domain used in the plots for Fig. 2.

must be a physical explanation, one which also can explain the wide range of delay times that have been observed.

It has been shown that slow slip events and aseismic creep can be dynamically triggered [Shelly et al., 2011; Wallace et al., 2018]. As slow slip events recently have been observed as precursors to large earthquakes [Ito et al., 2013; Kato et al., 2012; Meng et al., 2011; Kato and Nakagawa, 2014; Ruiz et al., 2014], perhaps triggered or enhanced precursory slow slip can account for delayed dynamic triggering [Peng and Gomberg, 2010; Shelly et al., 2011; Pollitz et al., 2014]. More specifically, propagating dynamic waves might rapidly push a gradually unlocking asperity closer to (but not in excess of) a failure threshold. Unfortunately, geodetic and seismic monitoring for the 2017 Mexico and 1992/1999 Southern California sequences were too sparse to directly observe such a process. Even if station coverage was dense, precursory slip and its response to dynamic waves may be below the resolution of most geophysics-based approaches. Numerical models can be used to overcome these limitations.

Previous numerical models and laboratory granular shear experiments have proven useful in the investigation of the delayed dynamic triggering mechanism [Griffa et al., 2012; Ferdowsi et al., 2015; Johnson and Jia, 2005; Gomberg et al., 1997]. Spring slider models governed by rate and state constitutive laws can reproduce the phenomenon of delayed dynamic triggering and show that the delay time between perturbation and subsequent triggered event is nonlinearly dependent on when in the loading cycle the perturbation is introduced [Gomberg et al., 1997]. Ferdowsi et al. (2015) reproduced the phenomenon of delayed triggering by introducing boundary-controlled perturbations into a 3D discrete element (DEM) assemblage undergoing stick-slip dynamics. Above a critical amplitude, the dynamic perturbations decreased the slipping contact ratio, shear modulus, and frictional strength of the granular gouge layer, hastening the time to failure. The numerical results are supported by granular laboratory experiments, in which shear modulus reduction caused by dynamic perturbations were shown to induce premature failure [Johnson and Jia, 2005]. These types of model approaches provide valuable insights into the mechanics and energy budget of triggered seismicity, yet they do not consider the complex interactions that arise within a full-scale segmented fault zone driven by far-field tectonic loading, which we believe to be relevant to the delayed triggering process.

Here, we use particle dynamics models to explore the possibility that slow slip can control delayed dynamic triggering on a megathrust fault interface. We consider a model in which the far field loading of a geometrically heterogeneous fault allows for the development of adjacent zones of strength (locked asperity) and weakness (slow slip). Our results lend support to the hypothesis of slow slip as a mechanism for delayed triggering [Pollitz et al., 2014; Shelly et al., 2011], and provide unique insights into the nonlinear relationship between timing of perturbation and delay period [Gomberg et al., 1997]. The model that we propose can also account for the wide-ranging delay times between causative and triggered seismicity observed in nature.

2. Methods

In this study, we use the discrete element method (DEM; Cundall and Strack, 1979) to simulate subduction zone earthquakes. DEM uses a time stepping, finite difference approach to solve Newton's equations of motion for every particle in a system in response to the contact and body forces acting on them. Particle contacts deform elastically, based on Hertz-Mindlin contact laws [Johnson, 1987]. A full description of RICEBAL, the code we implement here, can be found elsewhere [Morgan, 2015] and more details can be found in the Supplementary Material. In this suite of simulations, particles are assigned a shear modulus of 2.9 GPa, Poisson's ratio of 0.2, density of 2500 kg/m^2, and interparticle friction of 0.3. Each output of the simulation, which we refer to as "frame", is separated by sixty iterations of a 0.05 second time step, however we represent time in this study as a proportion of the interseismic loading cycle.

Our DEM model setup is designed to simulate the uppermost 60 km of a subduction zone undergoing tectonic loading (Fig. 1). To do this, ~100,000 particles of radius 60 m and 80 m are randomly generated within an 80 km by 40 km domain. During a consolidation phase, particles settle under the force of gravity. The pile of particles is then sculpted into the shape of a wedge by removing particles from the domain. We then apply interparticle bonds to create cohesive upper and lower plate units, which are separated by an unbonded interface that represents the megathrust fault. Bonds are not permanent in our implementation of the code and can break when they reach certain thresholds under tension and compression. This is analogous to off-fault damage that can occur in nature and may influence the distribution of earthquake energy during an event. Further details of the equations that govern bond breakage can be found in the Supplementary Material.

We define moving boundaries by controlling particle velocities within preset domains. To simulate tectonic loading, the base of the lower plate is held fixed while the left edge of the upper plate, or back wall, is displaced at a constant x-velocity. These fixed-velocity boundary units are shaded gray in Fig. 1. In response to the moving boundaries, strain localizes along the unbonded fault surface. A phase of fault preconditioning is carried out, in which back wall displacement is applied at 1 m/s until the entire length of the fault has undergone slip. After this preconditioning phase, we run the simulation for 600 total meters of back wall displacement at a reduced rate of 0.02 m/s.

A unique advantage of this setup is that geometrical irregularity naturally emerges and evolves as the simulated fault accumulates displacement. This emergent geometrical heterogeneity produces a wide range of realistic slip behaviors, including precursory slow slip and earthquakes of various size and complexity [Fournier and

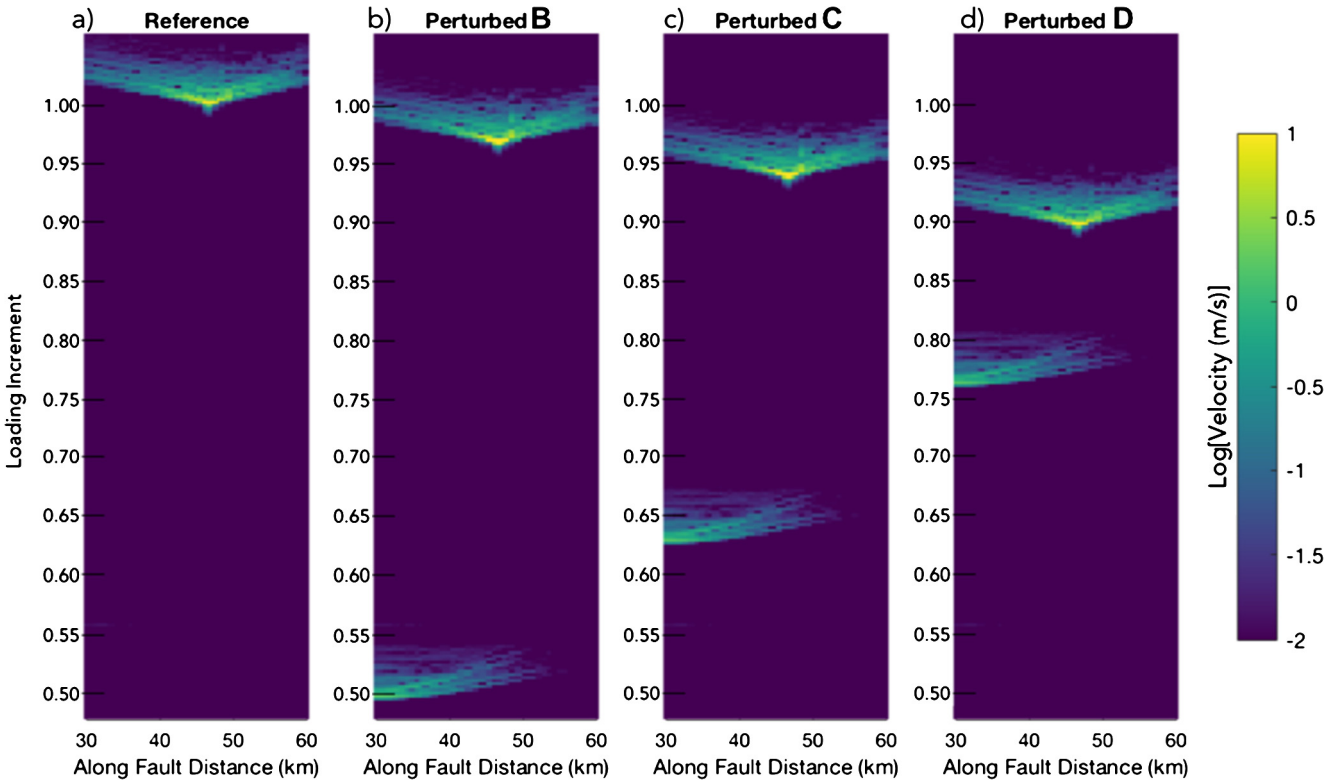

Fig. 2. Spatiotemporal fault slip maps. Colors represent logarithm of particle displacement rates within a 200 × 30000 meter domain located directly above the fault (dashed box, Fig. 1). **(a)** An earthquake nucleates at the end of the earthquake cycle (100% loading increment), under static loading boundary conditions. **(b, c, d)** Simulations B, C, and D are perturbed by a dynamic wave introduced at different times (loading increment 0.49, 0.63, 0.76, respectively). The resulting event is advanced in time relative to the Reference model, thus "triggered". Simulations A and E are not shown here, but can be seen in Fig. 4.

Morgan, 2012; Blank and Morgan, 2019; Caniven et al., 2019]. Furthermore, the geometrical irregularity compartmentalizes the fault, introducing zones that exhibit contrasting behaviors and interact in complex ways.

To test the hypothesis that slow precursory slip plays a critical role in delayed dynamic triggering, we must first reproduce the phenomenon. To do this, we compare earthquake behavior in six simulations restarted with identical parameters. One of the simulations is subjected only to the static loading boundary conditions (reference) while the other five are perturbed by dynamic waves. To separate the effects of static versus dynamic stress changes, we introduce a seismic perturbation by dropping a suspended particle, which falls under the force of gravity and impacts the wedge surface. Dynamic waves propagate from the point of impact, but upon their passing, leave the static stress state essentially unchanged. The transient mean stress change at the eventual point of triggered seismicity is ∼250 KPa (see Supplementary Material). This is higher than expected for remote waves in nature, but still within a reasonable range for near-field triggering. Because the models are deterministic and initiate from identical states, we can be certain that any deviations between the reference and perturbed models are a direct result of the imposed wave. The selected reference event is preceded by an interseismic quiescent period of 378 "frames". For the remainder of this paper, we represent time as a proportion of this 378-frame loading cycle, which we refer to as "loading increment".

3. Results

The timing of dynamic perturbations and event nucleation can be seen clearly in Fig. 2. Here, particle velocities within a 200 m × 30000 m domain above the fault (dashed box, Fig. 1) are scaled by color and stacked through time. Periods of fault locking appear dark blue whereas seismic velocities appear yellow. The four selected simulations presented in Fig. 2 are restarted from identical states amid a period of fault locking. In the absence of perturbation (Fig. 2, a), an event nucleates at loading increment 1.0, at 46.8 km along the fault. The event propagates bidirectionally and experiences peak slip velocities of ∼10 m/s. In simulations B, C, and D, perturbations related to the imposed waves intersect the fault at loading increment 0.497, 0.630, and 0.762, respectively (Figs. 2b, 2c, and 2d) and propagate from left to right. Subsequent earthquake nucleation for simulations B, C, and D occur at loading increment 0.955, 0.926, and 0.884, respectively, with source parameters almost identical to the reference event. "Clock advance" is defined here as the time difference between reference and triggered event and "delay" is the time difference between perturbation and triggered event. Simulated earthquakes A, B, C, D and E (A and E are not shown in Fig. 2) have clock advances of 0.016, 0.032, 0.063, 0.106, and 0.101 and delays of 0.603, 0.450, 0.288, 0.114, and 0.016 loading increments, respectively. Thus, perturbations introduced earlier in the interseismic period result in longer time delays and shorter clock advances. The time separation between perturbations in simulations A, B, C, and D (0.13 loading increments) is greater than the time separating their corresponding triggered events. Thus, our suite of simulations results in an inverse nonlinear relationship between timing of perturbation and clock advance.

To understand the cause of the observed temporal relationship, we analyze the conditions that lead to failure of the reference event itself. Fig. 3 shows the cumulative kinematic and stress changes that have developed between loading increment 0.34 and 0.87 (about 0.126 loading increments prior to the onset of the reference event). Cumulative displacement is calculated for each particle in the system and scaled by color (Fig. 3a). Relatively high displacements are observed near the back wall and decay toward

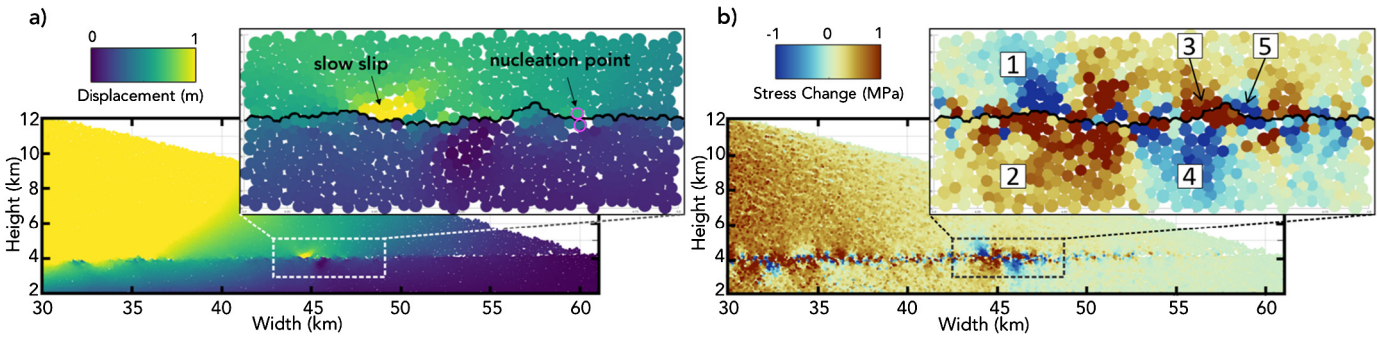

Fig. 3. Cumulative displacement and stress prior to rupture. (a) Cumulative displacement for the reference simulation between loading increment 0.34 and 0.87, for frontal fault domain denoted in Fig. 1, and enlarged display of domain centered around the future reference earthquake nucleation point (indicated by pink-outlined particles). **(b)** Total mean stress change for the reference simulation between loading increment 0.34 and 0.87, for the frontal domain, and enlarged domain centered around the future nucleation point. Numbers denote zones of gradual stress reduction (1,4,5) and enhancement (2,3) discussed in the text.

the toe. Lateral variability in displacement can be seen along the length of the fault. A zoomed view shows a small section along the fault with above average cumulative displacement of ∼1 m. This creeping segment lies ∼2.5 km to the left of the eventual nucleation point of the earthquake, denoted by the pink-highlighted pair of particles. The fault surface is traced by separating particles with positive (hanging wall) and negative (footwall) x-velocities prior to and during earthquake slip (see Supplemental Materials for more detail). The eventual nucleation point of the reference event lies ∼400 m trenchward of a geometric asperity with peak to trough relief of 192 meters.

Corresponding patterns observed in the displacement field are also seen in the particle mean stress change plots, which are derived by differencing two-dimensional stress tensors resolved at the particle centroids (σ_{ij}^{p}) (Cundall and Strack, 1983; Thornton and Barnes, 1986) as

$$\sigma_{ij}^{p} = \frac{1}{V_p}\left[\sum_{a=1}^{m}\left(r_i^a f_j^a\right)\right]_p$$

where V_p is the particle volume, m is the number of contact forces acting on the particle, r_i^a are the components of the particle radius normal to the contact, and f_j^a are the total forces acting in the jth direction. The particle mean stress is defined as,

$$\sigma_{mean}^{p} = \frac{\sigma_I + \sigma_{II}}{2}$$

where σ_I and σ_{II} are the maximum and minimum principle stresses, respectively. Fig. 3b shows the change in particle stresses that have developed between loading increments 0.34 and 0.87, where red colors represent stress increase and blue colors represent stress reduction. The average particle mean stress change within the entire system over this interval is 666.45 KPa. These positive stress changes are concentrated near the backwall and decay towards the toe. Heterogeneous stress change is evident along the fault and can be seen in detail in the zoomed domain. The previously identified creeping segment is bounded by several distinct areas of stress change. At its left edge, a zone of stress reduction (1) develops in the hanging wall, paired with a zone of stress rise in the footwall (2). To the right of the creeping segment, a zone of stress rise develops in the hanging wall (3) along with a zone of stress reduction in the footwall (4). The stress increase (3) develops along the left-hand side or "leading flank" of the aforementioned high relief asperity. On the right-hand side or "trailing flank" we observe a stress reduction (5). The future nucleation point of the reference event (outlined in pink) lies within the zone of stress decrease behind the geometrical asperity.

Average particle mean stress and absolute displacement are recorded within a 230 m × 270 m domain centered on the nucleation point (Zone 5 in Fig. 3). Stress is plotted against time (Fig. 4) and also average displacement (Fig. 4, inset top right), showing the reference (gray line) and perturbed simulations (colored lines). Over time, stress gradually decreases at the nucleation point in all six simulations. The rate of stress reduction in the reference model remains relatively constant until failure is reached at ∼632.6 MPa. In perturbed models A, B, C and D, the passing wave results in an immediate stress drop of ∼610 KPa. This dramatic initial change is then followed by a brief period (0.04–0.08 loading increments) of constant stress, or "stalled" rate of stress change. The gradual stress reduction then resumes, but at a lower rate than the reference. Through time, the difference between the perturbed and reference stress states in the nucleation zone, $\triangle\sigma$, decays. Perturbed model E fails 0.016 loading increments after the perturbation crosses the fault, and therefore represents triggering with very little delay time. Because it fails almost immediately after the perturbation, we do not observe any stalled or reduced rate of stress drop following the initial perturbation-induced stress reduction. The stress vs. displacement plot (Fig. 4, inset top right) shows that each model fails at nearly the same stress and displacement conditions, regardless of the temporal evolution of stress. The perturbed simulations deviate from the reference during and after perturbation, then gradually rejoin the reference state through time. A summary plot of clock advance and time delay as a function of timing of perturbation is shown in the bottom left inset of Fig. 4, which demonstrates that perturbations introduced progressively later in the loading cycle result in shorter time delays and longer clock advances. Perturbations introduced sufficiently late (i.e. model E) induce nearly instantaneous triggering, with clock advance equal to the reference nucleation time minus the perturbation time. In the case of instantaneous triggering, progressively later perturbations result in smaller clock advances (this accounts for the rollover in clock advance between simulations D and E in the summary plot).

4. Discussion

We see that earthquake nucleation in our models is preceded by a phase of stress reduction within the nucleation zone (Fig. 4), consistent with previous findings [Blank and Morgan, 2019]. The nucleation point itself, represented by the two pink particles in Fig. 5a, clarifies this phenomenon. For earthquake slip to initiate, the hanging wall particle must shift up and over the footwall particle. In so doing, fault-parallel contact forces are slowly reduced as the particles creep laterally and the fault zone dilates. We recognize that this nucleation point unlocking process is ubiquitous in our simulations of slip along irregular fault surfaces, providing important insights into nucleation processes along naturally rough faults [Blank and Morgan, 2019].

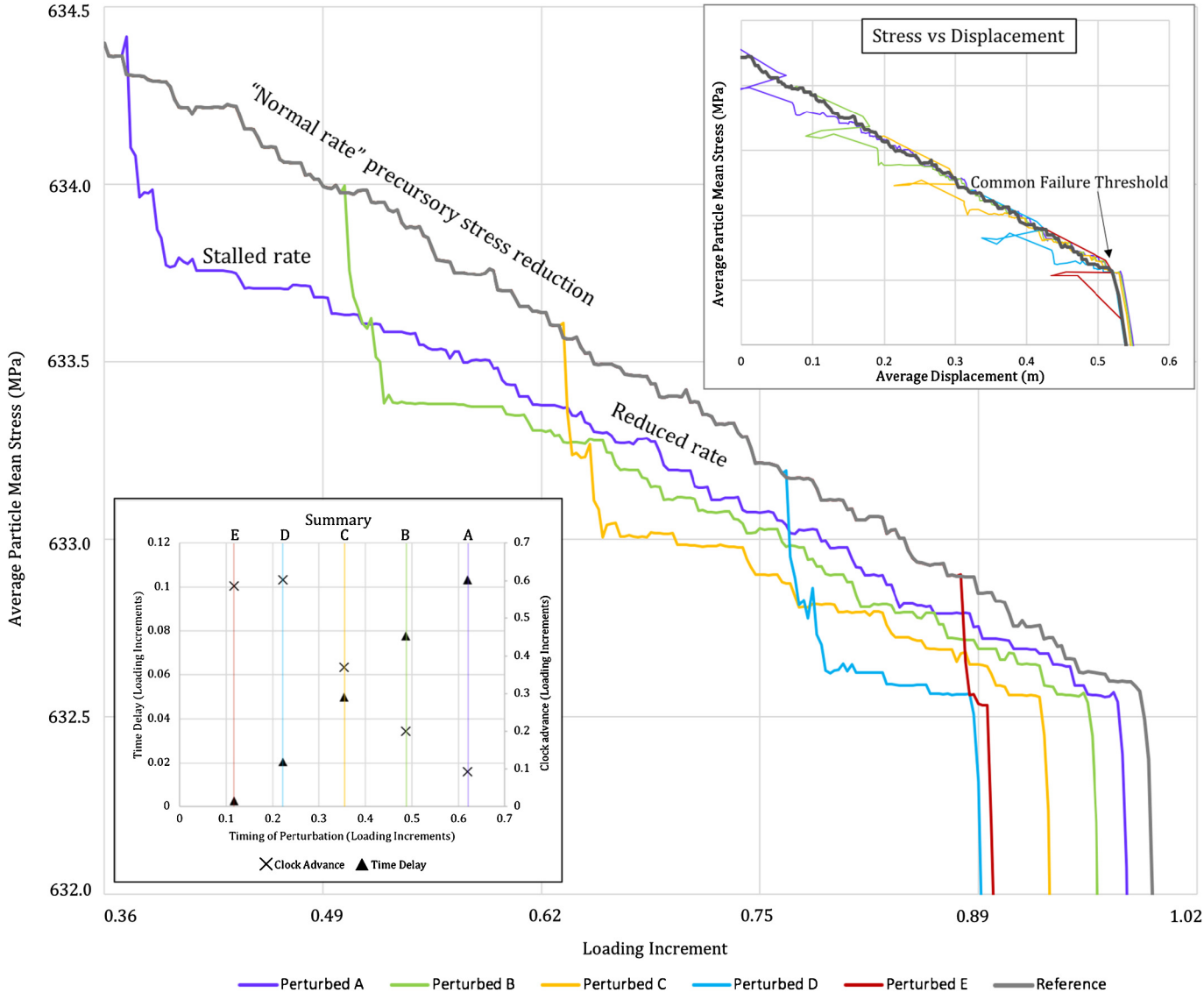

Fig. 4. Nucleation zone stress evolution. Average particle mean stress within the nucleation zone (Fig. 3b, zone 5) plotted through time for reference (gray) and perturbed simulations (colors). Failure occurs at similar stress conditions for all simulations. **Inset, top right.** Average mean stress for the six models, plotted against average displacement within nucleation zone. With the exception of simulation E, all models converge upon a similar stress-displacement path. **Inset, bottom left.** Summary plot of time delay (left y-axis, triangles) and clock advance (right y-axis, x-symbols) as a function of perturbation timing (x-axis), measured as the difference between perturbation time and reference earthquake nucleation time. Vertical colored lines correspond to perturbed simulations A-E.

Of greatest interest to this study, this nucleation point unlocking process also appears to be nested within a larger system of geometrically modulated aseismic slip and stress transfer, which introduce complex interacting processes. As we observe, approximately constant-rate slow slip takes place between about 44.5 km to 45 km along the fault (Fig. 5b, top panel), due to the relative mechanical weakness of this fault segment (see Supplemental Materials for how fault strength is determined). This slow slip is arrested at about 46 km along the fault, at the leading flank of a mechanically strong geometrical asperity. This serves as a buttress to the slow slip, resulting in the accumulation of stress along the leading flank of the asperity. Concurrently, stress is reduced along the trailing flank of the asperity. This defines a small stress shadow resulting from relative orientation of the trailing flank with the continuous tectonic loading stress. The future nucleation point is embedded within the stress reduction zone trailing the asperity (Fig. 5a). Apparently, the local reduction in stress facilitates lateral translation of the hanging wall over the footwall and fault dilation until the grain bridge collapses, resulting in earthquake slip.

The occurrence of dynamic perturbations accelerates the slow-slip modulated stress transfer process described above. The creeping zone responds to dynamic waves with relatively little resistance, allowing rapid stress transfer to the buttressing asperity, shifting the stress conditions at the nucleation point closer to failure ($\triangle\sigma$, Fig. 4). Immediately after the perturbation, slip in the creeping zones stalls while it catches up in the surrounding zones (annotated in Fig. 4 and Fig. 5b). As the system catches up, the slip velocity in the creeping zone increases from its stalled rate to a rate slightly less than that of the reference. Over time, the reference and perturbed simulations proceed toward failure at contrasting rates, gradually reducing the difference in nucleation zone stress state ($\triangle\sigma$). This process is nearly identical for all perturbed simulations, however the failure threshold is reached at different stages of the $\triangle\sigma$ reduction process, depending on when during the interseismic period the system was perturbed. This causes the nonlinear dependence between timing of perturbation and clock advance. This observation is consistent with results from spring slider models governed by rate and state constitutive laws [e.g.

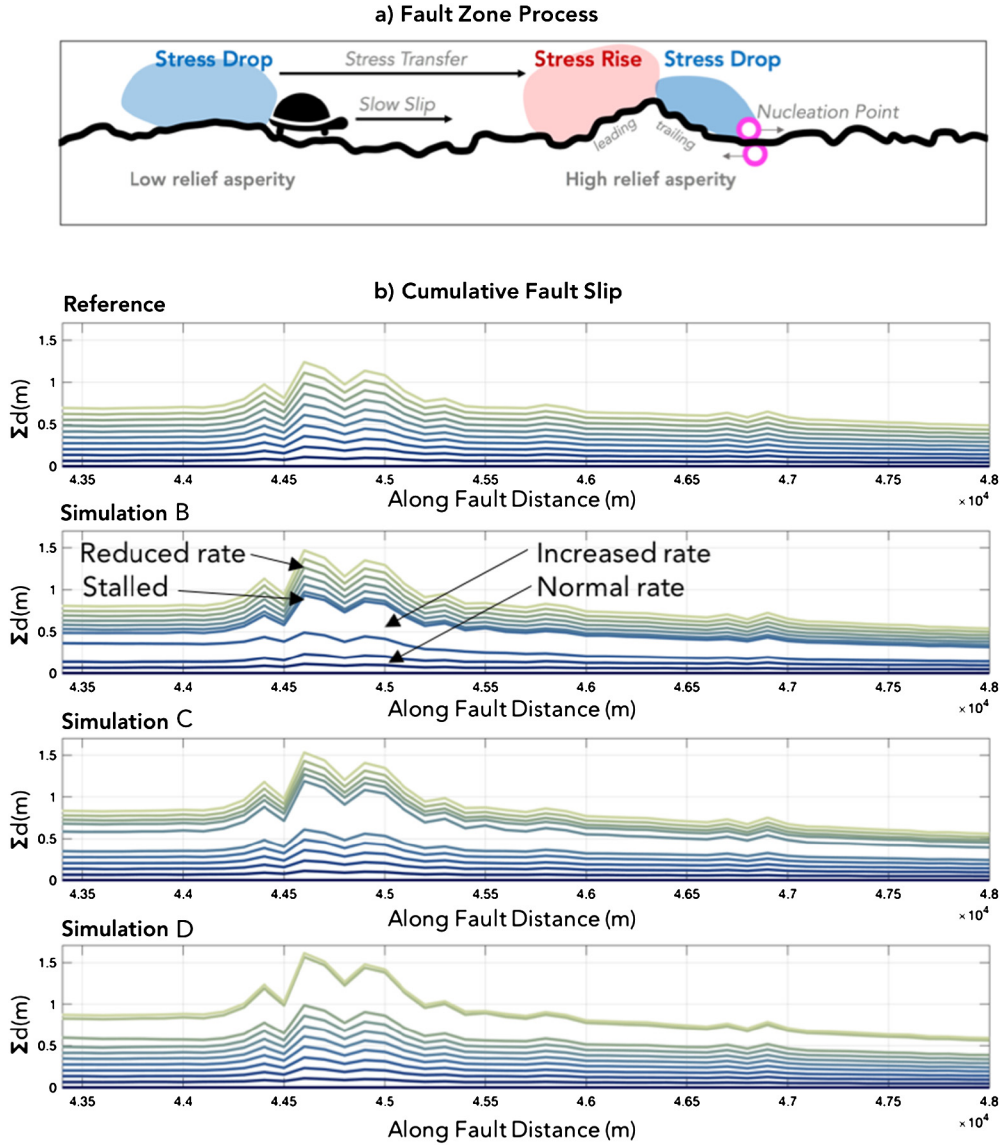

Fig. 5. Fault zone stress evolution and fault slip. (a) Irregular fault geometry creates low relief zones and high relief asperities. Slow slip in the low relief zone is accompanied by gradual stress decrease. Stress rise takes place on the leading flank of the high relief asperity, which is accompanied by stress reduction in a stress shadow along the trailing flank. The future nucleation point of the earthquake lies in the stress shadow, and experiences stress decrease prior to failure. **(b)** Pre-earthquake cumulative fault slip profiles for the reference and perturbed simulation B, C, and D between loading increment 0.34 and 0.87. Colored lines represent 0.05 loading increments. Displacement along the entire fault is increased due to perturbation and is highest along the slow slip patch. Slip rates following the perturbation induced initial increase, stall for ∼.05-.10 loading increments before resuming at a reduced rate.

Gomberg et al., 1997]. In our model, however, the dependence is explained by variable slip rates (and thus stress transfer) following the dynamic perturbation. As a simple test of perturbation magnitude dependence on $\triangle\sigma$ (and related clock advance), we ran a simulation with a smaller particle impactor. We observed a similar process with a smaller amount of stress reduction and clock advance (Supplementary Material S4).

Interestingly, the sequence described above defines a comprehensive model that can explain a wide range of triggering phenomena. For example, if the perturbing wave is introduced while the nucleation point is far from its failure threshold, the divergent stress states, defined by $\triangle\sigma$, could converge prior to nucleation, resulting in negligible clock advance, i.e., no apparent triggering (Simulation A). At the other extreme, (e.g. instantaneous triggering; Hill and Prejean, 2015; Peng and Gomberg, 2010; Parsons and Velasco, 2011; Parsons et al., 2012), if the perturbing wave is introduced when the nucleation point is close to failure, the induced rapid stress drop could trigger the earthquake almost instantly (Simulation E). Thus, these two end member behaviors bracket a continuum of behaviors that would produce delayed dynamic triggering of earthquakes. Spanning the continuum is an infinite range of potential clock advances made possible by the combination of a wide range of dynamic strain magnitudes (Fig. S4), and geometrical asperity stress conditions. The relatively uncommon occurrence of delayed triggering in nature may be due to the low likelihood that a dynamic perturbation will bring an asperity stress close to, but not at, its failure threshold. The aforementioned delayed triggering examples could fall along this continuum, with the Puebla/Chiapas event pair toward (but not at) the "instantaneous triggering" endmember and the Landers/Hector Mine event pair toward the "no apparent triggering" endmember.

A key underlying element of our proposed delayed triggering mechanism is local fault strength heterogeneity, which in our model is achieved through geometrical, and corresponding mechanical, segmentation of the fault. Geometrical asperities along the discrete fault surface respond to far field loading, causing some

segments to creep aseismically while others are locked. Because the weaker fault segment accumulates permanent strain in response to dynamic perturbation, and because slip in this weak zone is linked to the failure process in the adjacent locked zone, the path to failure is hastened. According to this hypothesis, a uniformly strong fault is unlikely to undergo significant precursory inelastic strain in response to a dynamic wave. Thus, once the transient perturbation has passed, the state of the fault would be unchanged, and failure would occur as usual, with no "memory" of the perturbation. In contrast, a fault that is uniformly weak would have no asperity to host stick slip behavior. Thus, the juxtaposition of weak slow slip zones and locked stick slip zones may be required for delayed triggering to occur. In nature, this segmentation could stem not only from geometrical, but frictional or rheological heterogeneity as well.

The insights gained from our suite of simulations underscore the significance of slow slip as a potential precursor for large earthquakes and confirm that it can be enhanced or triggered by propagating seismic waves [Pollitz et al., 2014; Shelly et al., 2011]. If true, our model has implications for seismic hazard assessment. Fault segments that exhibit enhanced signals of slow slip (e.g. increased tremor, geodetic displacement rates) in response to the seismic waves of a distant event might indicate high risk zones for future earthquakes. However, knowledge of the stress state and failure threshold at the site of the potential asperity remains required to predict the triggered seismicity in time. These quantities might be impossible to constrain in nature. As such, even if dynamically triggered or enhanced slow slip is identified, there is no guarantee that an associated earthquake is impending. This speaks to the broader question that exists in the earthquake community today: Is the size, location, and timing of an earthquake predetermined? In our deterministic model, by definition, they are. Nonetheless, emergent fault slip processes and their responses to perturbations are so complex that prediction is difficult even in our fully constrained 2D granular model. This problem of complexity is compounded in the real world, making precise predictions exceptionally difficult. Machine learning approaches might be well suited to identify how far an asperity is from failure in our model [Rouet-Leduc et al., 2017; Corbi et al., 2019, 2020]. This question is beyond the scope of the present study but can be addressed in future work.

Regardless of the predictability of triggered seismicity, our numerical results provide a unique window into the physical mechanism that controls delayed dynamic triggering. The results underscore the importance of along-fault heterogeneity and slow slip in the delayed triggering process. This is an element that should be considered in future earthquake models. Our results also suggest that delayed dynamic triggering is a common phenomenon, although only triggered event pairs with short delay periods are identifiable in nature.

5. Conclusions

The results of our suite of simulations are analogous to the phenomenon of delayed dynamic triggering observed in nature. The determinism of the model, along with access to detailed stress and displacement data, allows us to identify a causal connection between a perturbation and a triggered event. In our model, the passage of seismic waves causes a rapid advancement of prolonged precursory slow slip, which brings the eventual nucleation point near its failure threshold. This is consistent with the hypothesis of slow slip as a mechanism for delayed triggering [Shelly et al., 2011]. However, in our model, slow slip is enhanced rather than triggered by dynamic stress changes. Furthermore, this mechanism requires a segmented fault that is capable of hosting both slow and fast slip and depends upon the interactions between them. Finally, the delay between perturbing wave and triggered event is dependent not only on the magnitude of perturbation, but also the state of the triggered asperity. If true, this simple model can account for the wide range of delay times observed in nature and has relevant implications for seismic hazard assessment.

Declaration of competing interest

The authors declare that they have no known competing financial interests or personal relationships that could have appeared to influence the work reported in this paper.

Acknowledgements

This work was funded by National Science Foundation grant EAR–1723249. Computing facilities were made available in part through the Rice Center for Computational Geophysics. We thank two anonymous reviewers for their insights which greatly improved the quality of this work.

Appendix A. Supplementary material

Supplementary material related to this article can be found online at https://doi.org/10.1016/j.epsl.2020.116695.

References

Alberto, Yolanda, et al., 2018. Reconnaissance of the 2017 Puebla, Mexico earthquake. Soil Found. 58 (5), 1073–1092.

Blank, D.G., Morgan, J.K., 2019. Precursory stress changes and fault dilation lead to fault rupture: insights from discrete element simulations. Geophys. Res. Lett. 46 (6), 3180–3188. https://doi.org/10.1029/2018GL081007.

Brodsky, Emily E., van der Elst, Nicholas J., 2014. The uses of dynamic earhquake triggering.

Caniven, Yannick Pierre, et al., 2019. DEM simulations of earthquake cycles along strike-slip faults: controls on the slow-slip nucleation of earthquakes. AGUFM 2019, S21F-0572.

Corbi, Fabio, et al., 2019. Machine learning can predict the timing and size of analog earthquakes. Geophys. Res. Lett. 46 (3), 1303–1311.

Corbi, Fabio, et al., 2020. Predicting imminence of analog megathrust earthquakes with Machine Learning: implications for monitoring subduction zones. Geophys. Res. Lett. 47 (7), e2019GL086615.

Cundall, Peter A., Strack, Otto D.L., 1979. A discrete numerical model for granular assemblies. Geotechnique 29 (1), 47–65.

Cundall, P.A., Strack, O.D.L., 1983. Modeling of microscopic mechanisms in granular materials. In: Jenkins, J.T., Satake, M. (Eds.), Mechanics of Granular Materials: New Models and Constitutive Relations. Elsevier, New York, pp. 137–149.

Felzer, Karen R., et al., 2002. Triggering of the 1999 Mw 7.1 Hector Mine earthquake by aftershocks of the 1992 Mw 7.3 Landers earthquake. J. Geophys. Res., Solid Earth 107 (B9), ESE-6.

Ferdowsi, Behrooz, et al., 2015. Acoustically induced slip in sheared granular layers: application to dynamic earthquake triggering. Geophys. Res. Lett. 42 (22), 9750–9757.

Fournier, T., Morgan, J., 2012. Insights to slip behavior on rough faults using discrete element modeling. Geophys. Res. Lett. 39 (12). https://doi.org/10.1029/2012GL051899.

Freed, Andrew M., 2005. Earthquake triggering by static, dynamic, and postseismic stress transfer. Annu. Rev. Earth Planet. Sci. 33, 335–367.

Gomberg, Joan, Johnson, Paul, 2005. Dynamic triggering of earthquakes. Nature 437 (7060), 830.

Gomberg, Joan, Blanpied, Michael L., Beeler, N.M., 1997. Transient triggering of near and distant earthquakes. Bull. Seismol. Soc. Am. 87 (2), 294–309.

Gomberg, J., et al., 2001. Earthquake triggering by seismic waves following the Landers and Hector Mine earthquakes. Nature 411 (6836), 462–466.

Gomberg, Joan, Bodin, Paul, Reasenberg, Paul A., 2003. Observing earthquakes triggered in the near field by dynamic deformations. Bull. Seismol. Soc. Am. 93 (1), 118–138.

Gomberg, J., et al., 2004. Earthquake nucleation by transient deformations caused by the M = 7.9 Denali, Alaska, earthquake. Nature 427 (6975), 621–624.

Griffa, M., et al., 2012. Meso-mechanical analysis of deformation characteristics for dynamically triggered slip in a granular medium. Philos. Mag. 92 (28–30), 3520–3539.

Harris, Ruth A., 1998. Introduction to special section: stress triggers, stress shadows, and implications for seismic hazard. J. Geophys. Res., Solid Earth 103 (B10), 24347–24358.

Hill, David P., Prejean, Stephanie, 2015. Dynamic triggering, pp. 273–304.
Hill, David P., et al., 1993. Seismicity remotely triggered by the magnitude 7.3 Landers, California, earthquake. Science 260 (5114), 1617–1623.
Hodge, Michael, Fagereng, Å., Biggs, J., 2018. The role of coseismic Coulomb stress changes in shaping the hard link between normal fault segments. J. Geophys. Res., Solid Earth 123 (1), 797–814.
Ito, Yoshihiro, et al., 2013. Episodic slow slip events in the Japan subduction zone before the 2011 Tohoku-Oki earthquake. Tectonophysics 600, 14–26.
Jaeger, J.C., Cook, N.G.W., Zimmerman, R., 1979. Rock mechanics. In: Fundamentals of Rock Mechanics.
Johnson, Christopher W., Bürgmann, Roland, 2016. Delayed dynamic triggering: local seismicity leading up to three remote M $\geq$ 6 aftershocks of the 11 April 2012 M8.6 Indian Ocean earthquake. J. Geophys. Res., Solid Earth 121 (1), 134–151.
Johnson, Kenneth Langstreth, 1987. Contact Mechanics. Cambridge University Press.
Johnson, Paul A., Jia, Xiaoping, 2005. Nonlinear dynamics, granular media and dynamic earthquake triggering. Nature 437 (7060), 871–874.
Kato, Aitaro, Nakagawa, Shigeki, 2014. Multiple slow-slip events during a foreshock sequence of the 2014 Iquique, Chile Mw 8.1 earthquake. Geophys. Res. Lett. 41 (15), 5420–5427.
Kato, Aitaro, et al., 2012. Propagation of slow slip leading up to the 2011 Mw 9.0 Tohoku-Oki earthquake. Science 335 (6069), 705–708.
Kilb, Deborah, Gomberg, Joan, Bodin, Paul, 2000. Triggering of earthquake aftershocks by dynamic stresses. Nature 408 (6812), 570–574.
Kilb, Debi, Gomberg, Joan, Bodin, Paul, 2002. Aftershock triggering by complete Coulomb stress changes. J. Geophys. Res., Solid Earth 107 (B4), ESE-2.
King, Geoffrey C.P., Stein, Ross S., Lin, Jian, 1994. Static stress changes and the triggering of earthquakes. Bull. Seismol. Soc. Am. 84 (3), 935–953.
Meng, Lingsen, Inbal, Asaf, Ampuero, Jean-Paul, 2011. A window into the complexity of the dynamic rupture of the 2011 Mw 9 Tohoku-Oki earthquake. Geophys. Res. Lett. 38, 7.
Morgan, J., 2015. Effects of cohesion on the structural and mechanical evolution of fold and thrust belts and contractional wedges: discrete element simulations. J. Geophys. Res., Solid Earth 120. https://doi.org/10.1002/2014JB011455.
Parsons, Tom, 2005. A hypothesis for delayed dynamic earthquake triggering. Geophys. Res. Lett. 32, 4.
Parsons, Tom, Velasco, Aaron A., 2011. Absence of remotely triggered large earthquakes beyond the mainshock region. Nat. Geosci. 4 (5), 312–316.
Parsons, Tom, et al., 2012. Unraveling the apparent magnitude threshold of remote earthquake triggering using full wavefield surface wave simulation. Geochem. Geophys. Geosyst. 13 (6).
Peng, Zhigang, Gomberg, Joan, 2010. An integrated perspective of the continuum between earthquakes and slow-slip phenomena. Nat. Geosci. 3 (9), 599–607.
Pollitz, Fred F., et al., 2014. The profound reach of the 11 April 2012 M 8.6 Indian Ocean earthquake: short-term global triggering followed by a longer-term global shadow. Bull. Seismol. Soc. Am. 104 (2), 972–984.
Rouet-Leduc, Bertrand, et al., 2017. Machine learning predicts laboratory earthquakes. Geophys. Res. Lett. 44 (18), 9276–9282.
Ruiz, S., et al., 2014. Intense foreshocks and a slow slip event preceded the 2014 Iquique Mw 8.1 earthquake. Science 345 (6201), 1165–1169.
Segou, Margarita, Parsons, Tom, 2018. Testing earthquake links in Mexico from 1978 to the 2017 M = 8.1 Chiapas and M = 7.1 Puebla shocks. Geophys. Res. Lett. 45 (2), 708–714.
Shelly, David R., et al., 2011. Triggered creep as a possible mechanism for delayed dynamic triggering of tremor and earthquakes. Nat. Geosci. 4 (6), 384–388.
Stein, Ross S., 1999. The role of stress transfer in earthquake occurrence. Nature 402 (6762), 605–609.
Thornton, C., Barnes, D.J., 1986. Computer simulated deformation of compact granular assemblages. Acta Mech. 64, 45–61.
Toda, S., Stein, R.S., 2017. The September 2017 M = 8.1 Chiapas and M = 7.1 Puebla, Mexico, earthquakes: chain reaction or coincidence? In: AGU Fall Meeting Abstracts.
Wallace, Laura M., et al., 2017. Large-scale dynamic triggering of shallow slow slip enhanced by overlying sedimentary wedge. Nat. Geosci. 10 (10), 765–770.
Wallace, Laura M., et al., 2018. Triggered slow slip and afterslip on the southern Hikurangi subduction zone following the Kaikōura earthquake. Geophys. Res. Lett. 45 (10), 4710–4718.
Walter, Jacob I., et al., 2015. Far-field triggering of foreshocks near the nucleation zone of the 5 September 2012 (MW 7.6) Nicoya Peninsula, Costa Rica earthquake. Earth Planet. Sci. Lett. 431, 75–86.
Zeng, Yuehua, 2001. Viscoelastic stress-triggering of the 1999 Hector Mine earthquake by the 1992 Landers earthquake. Geophys. Res. Lett. 28 (15), 3007–3010.